

# PTS-SNN: A Prompt-Tuned Temporal Shift Spiking Neural Networks for Efficient Speech Emotion Recognition

Xun Su, Huamin Wang, Qi Zhang

**Abstract**—Speech Emotion Recognition (SER) is widely deployed in Human-Computer Interaction, yet the high computational cost of conventional models hinders their implementation on resource-constrained edge devices. Spiking Neural Networks (SNNs) offer an energy-efficient alternative due to their event-driven nature; however, their integration with continuous Self-Supervised Learning (SSL) representations is fundamentally challenged by distribution mismatch, where high-dynamic-range embeddings degrade the information coding capacity of threshold-based neurons. To resolve this, we propose Prompt-Tuned Spiking Neural Networks (PTS-SNN), a parameter-efficient neuromorphic adaptation framework that aligns frozen SSL backbones with spiking dynamics. Specifically, we introduce a Temporal Shift Spiking Encoder to capture local temporal dependencies via parameter-free channel shifts, establishing a stable feature basis. To bridge the domain gap, we devise a Context-Aware Membrane Potential Calibration strategy. This mechanism leverages a Spiking Sparse Linear Attention module to aggregate global semantic context into learnable soft prompts, which dynamically regulate the bias voltages of Parametric Leaky Integrate-and-Fire (PLIF) neurons. This regulation effectively centers the heterogeneous input distribution within the responsive firing range, mitigating functional silence or saturation. Extensive experiments on five multilingual datasets (e.g., IEMOCAP, CASIA, EMODB) demonstrate that PTS-SNN achieves 73.34% accuracy on IEMOCAP, comparable to competitive Artificial Neural Networks (ANNs), while requiring only 1.19M trainable parameters and 0.35 mJ inference energy per sample.

**Index Terms**—Spiking Neural Networks, Speech Emotion Recognition, Prompt Tuning, Energy Efficiency, Neuromorphic Adaptation.

## I. INTRODUCTION

**S**PEECH Emotion Recognition (SER) is fundamental to Human-Computer Interaction (HCI), enabling embodied agents to perceive emotional states and interpret human intent [1]. Although feature extraction has evolved from handcrafted descriptors [2] to Self-Supervised Learning (SSL) representations [3], state-of-the-art systems typically employ dense Artificial Neural Networks (ANNs) for downstream inference. These architectures, however, incur high computational costs and memory overheads [4], limiting their deployment on resource-constrained edge devices [5]. In this context, Spiking Neural Networks (SNNs) offer an energy-efficient alternative [6]. By leveraging biological membrane potential dynamics and sparse, event-driven computation, SNNs naturally model temporal evolution while significantly reducing power consumption [7].

While combining continuous representation learning with discrete event-driven dynamics holds theoretical value, the

inherent heterogeneity in their information coding mechanisms presents substantial adaptation challenges [6]. Empirical observation indicates that directly applying SNNs to self-supervised features results in performance degradation [8]. The fundamental obstacle is the feature distribution shift between upstream continuous representations and downstream spiking neurons [7], [9]. Specifically, pre-trained embedding vectors typically exhibit high dynamic ranges and dense manifold distributions, whereas Leaky Integrate-and-Fire (LIF) [10] neurons function as threshold-based filters sensitive to input intensity [11]. Without targeted calibration, high-variance feature streams drive neurons into two extreme states: functional silence caused by weak inputs or firing saturation triggered by excessive signals [12], as visualized in Figure 1. Both extremes disrupt the sparse temporal coding mechanism required for effective feature integration [13].

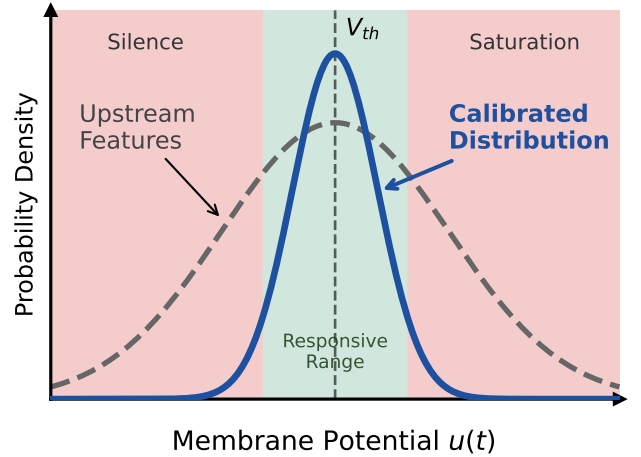


**Fig. 1: Illustration of the Distribution Mismatch.** The raw Upstream Features (dashed grey curve) exhibit a high dynamic range that extends significantly into the Silence or Saturation zones (red regions), causing information loss. In contrast, the proposed PTS-SNN realigns these features into a Calibrated Distribution (solid blue curve) concentrated within the Responsive Range (green region) around the firing threshold  $V_{th}$ , thereby maximizing the temporal coding capacity of spiking neurons.

To address the feature distribution mismatch between continuous representations and discrete dynamics [9], we propose PTS-SNN, a neuromorphic adaptation framework. Instead of modifying the massive pre-trained backbone [14], our approach aligns the frozen continuous features with discrete spiking dynamics through a two-stage calibration process. First, we introduce a Temporal Shift Spiking Encoder, which employs parameter-free channel shifts to capture local temporal dependencies [15]. This stabilizes the high-frequency

Xun Su, Huamin Wang, and Qi Zhang are with College of Artificial Intelligence, Southwest University, Chongqing, 400715, China, and also with Chongqing Key Laboratory of Brain Inspired Computing and Intelligent Chips, Chongqing, 400715, China (e-mail:swuring@email.swu.edu.cn; hmwang@swu.edu.cn; myhonor151@email.swu.edu.cn)

fluctuations in the raw feature manifold, providing a robust input basis. Crucially, to resolve the threshold sensitivity issue, we devise a Context-Aware Membrane Potential Calibration strategy based on Spiking Sparse Linear Attention [16]. This mechanism aggregates global semantic context into learnable soft prompts [17], [18], which then generate dynamic bias voltages to actively regulate the baseline potential of Parametric Leaky Integrate-and-Fire (PLIF) neurons [19]. This bio-inspired regulation effectively centers the heterogeneous input distribution within the responsive firing range, mitigating the risk of functional silence or saturation. The contributions of this paper can be summarized as follows:

(1) We propose PTS-SNN, a parameter-efficient neuromorphic adaptation framework designed to resolve the feature distribution mismatch between continuous SSL representations and discrete spiking dynamics. By integrating a Temporal Shift Spiking Encoder with Spiking Sparse Linear Attention, the architecture efficiently constructs a robust feature space while keeping the upstream backbone frozen.

(2) We introduce a Context-Aware Membrane Potential Calibration strategy inspired by biological homeostatic regulation. Unlike traditional semantic tokens, our learnable soft prompts function as active regulators that generate dynamic bias voltages. This mechanism aligns heterogeneous feature distributions with the sensitive response range of PLIF neurons, effectively preventing firing silence or saturation.

(3) We validate the model on five multilingual datasets (IEMOCAP, CASIA, EMODB, EMOVO, and URDU). Experimental results demonstrate that PTS-SNN achieves competitive accuracy (73.34% on IEMOCAP) against state-of-the-art ANNs while requiring only 1.19 M parameters and 0.35 mJ inference energy per sample, verifying its potential for energy-constrained edge intelligence.

The structure of this paper is as follows. Section II reviews related work in SSL and SNNs. Section III formulates the distribution mismatch problem and details the proposed PTS-SNN framework, specifically focusing on the temporal shift encoder and context-aware potential calibration. Section IV evaluates the model’s performance and energy efficiency across five multilingual benchmarks, followed by conclusions in Section V.

## II. RELATED WORKS

### A. Self-Supervised Learning in Speech Emotion Recognition

Early SER primarily relied on handcrafted acoustic features such as MFCCs and eGeMAPS [2]. While computationally efficient, these static descriptors struggle to capture the hierarchical temporal dependencies inherent in complex emotional expressions [1]. Recently, SSL has emerged as a dominant paradigm for feature extraction [20]. Pre-trained frameworks like Wav2Vec 2.0 [21] and the domain-specific emotion2vec [22] leverage large-scale unlabeled data to learn robust contextual representations, exhibiting superior generalization compared to traditional baselines [23].

However, adapting these models to downstream tasks typically necessitates full fine-tuning or the attachment of dense

ANN decoders [24]. These strategies introduce high parameter redundancy and inference latency, hindering deployment on resource-limited edge devices [25]. More critically, the dense floating-point matrix multiplications inherent in ANNs are fundamentally incompatible with the asynchronous, sparse paradigm of neuromorphic computing [26]–[28]. Consequently, developing lightweight adaptation strategies that align frozen SSL features with spiking dynamics remains a critical research challenge [29], [30].

### B. Spiking Neural Networks for Audio Processing

SNNs utilize an event-driven paradigm to minimize computational energy, making them intrinsically suitable for audio processing [31], [32]. Recent advancements have scaled these architectures to complex tasks such as Keyword Spotting [33] and Large Vocabulary Continuous Speech Recognition [4], [34]. In the domain of SER, hybrid architectures—typically employing Convolutional Neural Networks (CNNs) as front-ends—have been developed to extract features for spiking backends [35], [36]. These approaches exploit spiking temporal dynamics to capture emotional prosody [37] while maintaining low computational overhead.

However, existing SNN-based emotion recognition models remain constrained by their input representations, predominantly relying on low-level acoustic features such as MFCCs or spectrograms [38], [39]. While hybrid CNN-SNN architectures demonstrate efficacy in mining local patterns—achieving an accuracy of approximately 65.3% on standard six-class benchmarks [40], which is comparable to traditional ANNs—they are fundamentally limited by the inherent semantic ceiling of shallow acoustic descriptors [1]. Consequently, they fail to capture the deep, high-level emotional cues that advanced ANN systems extract via SSL [22], [23]. The core challenge, therefore, is not the fitting capability of the network, but the effective integration of deep continuous representations with discrete neuromorphic dynamics [7]. The primary obstacle lies in the distributional heterogeneity between pre-trained manifolds and spiking thresholds, which necessitates targeted adaptation strategies to realize high-performance, energy-efficient recognition [41].

### C. Prompt learning and adaptation techniques

Prompt Learning, originally developed for Natural Language Processing (NLP) [42], has emerged as a dominant strategy for Parameter-Efficient Fine-Tuning (PEFT) [43]. By optimizing a small set of trainable vectors while keeping the pre-trained backbone frozen [44], this paradigm effectively adapts foundation models to downstream tasks with minimal computational overhead [14]. Recent studies have successfully extended this methodology to computer vision [45] and audio processing [46], validating its efficacy in mitigating cross-modal distribution shifts [46], [47].

Despite these successes, the integration of prompt tuning into Neuromorphic Computing remains limited. Although recent works strive to enhance SNN representational power [48], [49], existing optimization strategies primarily focus on surrogate gradient learning [50] or ANN-to-SNN conversion

[51]. While hybrid architectures attempt to bridge the gap, they are often constrained by shallow acoustic inputs, limiting semantic depth [52], [53]. Consequently, there is a lack of efficient adaptation protocols for pre-trained continuous representations [54]. The fundamental obstacle lies in a mechanistic incompatibility: standard prompts function as continuous additive vectors [43], which are distinct from the discrete, threshold-based firing dynamics of SNNs [55]. Directly injecting continuous prompts into binary spike sequences disrupts the precise timing required for temporal coding [56], leading to information loss.

To resolve this, we propose a biophysical reformulation of prompting tailored for SNNs. Distinct from semantic tokens used in ANNs, we model prompts as homeostatic regulation signals akin to biological control mechanisms [57]. By mapping learnable vectors to dynamic bias voltages, this method actively calibrates the baseline membrane potential [17]. This strategy achieves precise alignment between continuous upstream features and discrete neuronal response ranges without restructuring the underlying network [54], offering a parameter-efficient solution to the feature distribution mismatch.

### III. METHODS

#### A. Problem Formulation

**Task Definition.** Let  $\mathcal{D} = \{(\mathbf{z}_i, y_i)\}_{i=1}^N$  denote the labeled dataset, where  $\mathbf{z}_i \in \mathcal{Z}$  represents the raw speech waveform and  $y_i \in \mathcal{Y} = \{1, \dots, K\}$  is the corresponding categorical emotion label. We employ a pre-trained SSL model (emotion2vec) as the feature extractor, denoted by mapping function  $f_{\text{ssl}} : \mathcal{Z} \rightarrow \mathbb{R}^{T \times D_{in}}$ . To maintain parameter efficiency, the backbone parameters  $\Theta_{\text{ssl}}$  are frozen. Consequently, for each sample  $\mathbf{z}$ , we obtain a deterministic continuous representation sequence  $\mathbf{X} \in \mathbb{R}^{T \times D_{in}}$ , where  $T$  is the sequence length and  $D_{in}$  is the channel dimension.

**Neuronal Dynamics.** The downstream classifier is constructed using PLIF neurons. Unlike standard LIF models with fixed hyperparameters, PLIF neurons incorporate a learnable membrane time constant to adaptively model temporal dependencies. Let  $u_j^{(l)}[t]$  and  $s_j^{(l)}[t]$  denote the membrane potential and spike output of the  $j$ -th neuron in layer  $l$  at time step  $t$ , respectively. The discrete-time dynamics are governed by the following difference equation:

$$u_j^{(l)}[t] = \tau_j^{(l)} \cdot u_j^{(l)}[t-1] + i_j^{(l)}[t] - V_{th} \cdot s_j^{(l)}[t-1] \quad (1)$$

where  $i_j^{(l)}[t]$  is the synaptic input current,  $V_{th}$  is the firing threshold, and  $\tau_j^{(l)} \in (0, 1)$  represents the learnable decay factor. The spike generation follows the Heaviside step function  $\Theta(\cdot)$ :

$$s_j^{(l)}[t] = \Theta(u_j^{(l)}[t] - V_{th}) \quad \text{s.t.} \quad s_j^{(l)}[t] \in \{0, 1\} \quad (2)$$

**Distribution Mismatch.** A fundamental compatibility barrier exists between the continuous manifold of  $\mathbf{X}$  and the discrete switching dynamics of Eq. (2). The pre-trained features often exhibit a high dynamic range, leading to a distribution

shift against the fixed threshold  $V_{th}$ . We formulate this as two pathological states for the synaptic current  $\mathbf{I}$ :

$$\begin{cases} \mathbb{E}_t[\mathbf{I}[t]] \ll V_{th} \implies \sum_{t=1}^T s[t] \rightarrow 0 \\ \mathbb{E}_t[\mathbf{I}[t]] \gg V_{th} \implies \sum_{t=1}^T s[t] \rightarrow T \end{cases} \quad (3)$$

Both extremes minimize the entropy of the spike train  $H(\mathbf{S})$ , thereby degrading the temporal coding capacity of the SNN.

**Learning Goal.** To resolve the distribution mismatch, we propose a learnable neuromorphic adapter  $\mathcal{G}_\theta : \mathbb{R}^{T \times D_{in}} \rightarrow \mathbb{R}^{T \times D_{out}}$ . The objective is to map the continuous input  $X$  to a calibrated latent space aligned with the receptive field of the PLIF classifier  $\mathcal{F}_\phi$ . The predicted class probability distribution  $\hat{y}$  is obtained by decoding the mean firing rate of the output neurons over  $T$  steps:

$$\hat{y} = \text{Softmax} \left( \frac{1}{T} \sum_{t=1}^T \mathcal{F}_\phi(\mathcal{G}_\theta(X)[t]) \right) \quad (4)$$

Our goal is to jointly optimize the adapter parameters  $\theta$  and SNN weights  $\phi$  to minimize the discrepancy between  $\hat{y}$  and the ground truth  $y$ . The specific loss function design, which addresses class imbalance and label noise, is detailed in Section III.F.

#### B. Overall architecture

As illustrated in Figure 2, we present PTS-SNN, a parameter-efficient framework designed to reconcile continuous SSL representations with discrete spiking dynamics. By freezing the pre-trained emotion2vec backbone, the architecture optimizes only a lightweight adapter to transform static features into dynamic spike sequences through three cascaded stages.

First, the Temporal Shift Spiking Encoder employs parameter-free channel shift operations within residual spiking blocks. This module captures local temporal dependencies and smooths high-frequency fluctuations in the feature manifold to establish a stable input basis.

Subsequently, the Spiking Sparse Linear Attention (SSLA) module integrates learnable soft prompts with the feature sequence. SSLA executes a linear interaction to aggregate global semantic context into prompt vectors, simultaneously leveraging neuronal thresholds to filter background redundancy.

Finally, the context-rich prompts drive the Homeostatic Bias Generator. Inspired by biological regulation, this component generates dynamic voltage biases that shift the baseline potential, proactively aligning the heterogeneous input distribution with the PLIF backend's sensitive response range for effective spike decoding.

#### C. Temporal Shift Spiking Encoder

Raw feature sequences derived from the frozen backbone typically exhibit frame-level independence and high-amplitude outliers. These characteristics lack explicit modeling of short-term prosody and can destabilize the firing dynamics of downstream neurons. To mitigate these issues, we construct the Temporal Shift Spiking Encoder. This module functions to

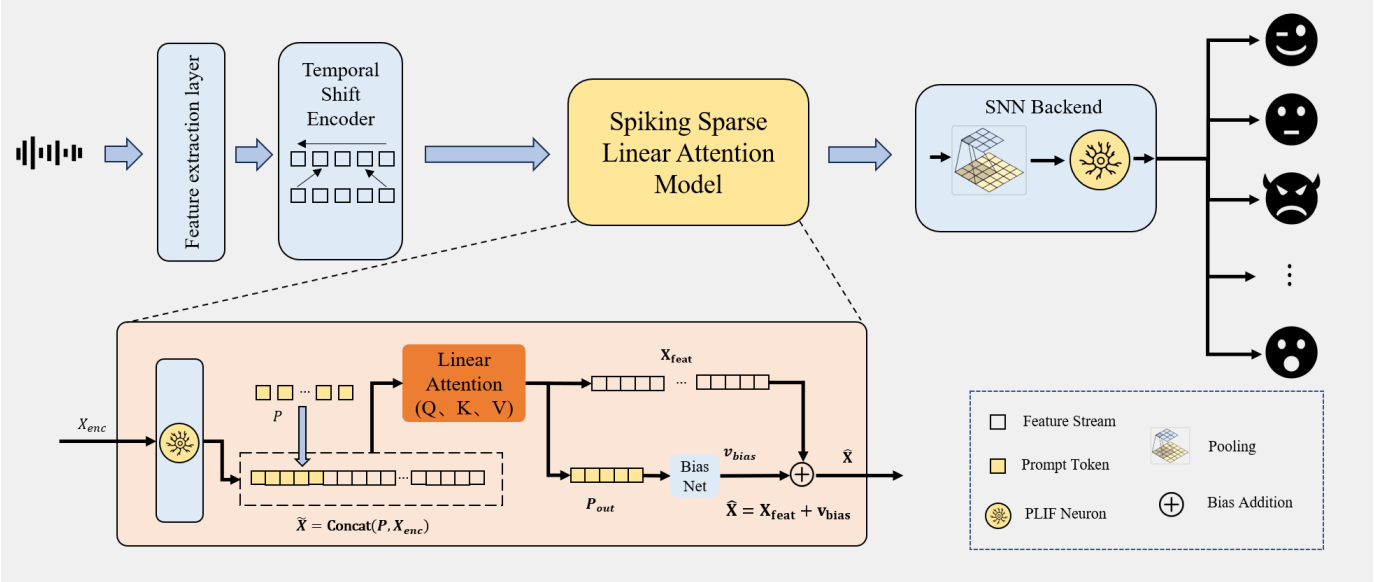


Fig. 2: **Overview of the proposed PTS-SNN framework.** The architecture processes features from a frozen backbone through three cascaded stages: the Temporal Shift Spiking Encoder for capturing local dependencies via parameter-free shifts, the SSLA module for aggregating global semantic context, and the SNN Backend for emotion classification. The bottom panel details the SSLA mechanism, where learnable soft prompts interact with sparse spike maps to generate dynamic voltage biases for membrane potential calibration.

smooth the input manifold and extract compact local context through two key stages: soft saturation preprocessing and efficient temporal shifting.

**Soft Saturation Preprocessing.** To prevent numerical instability, we first constrain the dynamic range of the input features  $X \in \mathbb{R}^{T \times D}$ . We design a soft saturation function that combines Layer Normalization with a scaled hyperbolic tangent transformation:

$$X_{pre} = \tanh(\xi \cdot \text{LayerNorm}(X)) \quad (5)$$

We empirically set the scaling factor  $\xi$  to 0.1. Unlike hard clipping, this differentiable operation smoothly compresses extreme outliers into a linear region. It ensures that the input current remains within a stable range suitable for neuromorphic computing while preserving the gradient flow required for backpropagation.

**Spiking Temporal Shift Blocks.** The preprocessed sequence  $X_{pre}$  enters an encoding network composed of two cascaded residual spiking blocks. This network progressively reduces the feature dimension ( $768 \rightarrow 512 \rightarrow 256$ ) to filter redundancy. Within each block, we replace standard convolutional kernels with a parameter-free Temporal Shift operation. By shifting a fraction of feature channels along the temporal axis, this mechanism facilitates information exchange between adjacent frames with zero floating-point operations (FLOPs) as illustrated in Figure 3. The computational flow for the  $l$ -th block is formalized as:

$$H^{(l)} = \text{PLIF}(\text{BN}(W^{(l)}(\text{Shift}(H^{(l-1)})) + b^{(l)})) \quad (6)$$

Here,  $W^{(l)}$  and  $b^{(l)}$  denote the weights and biases of the linear projection. The Shift operation explicitly captures local temporal dependencies, providing the PLIF neurons with context-aware input currents. The learnable time constants of the PLIF neurons further optimize the integration of these

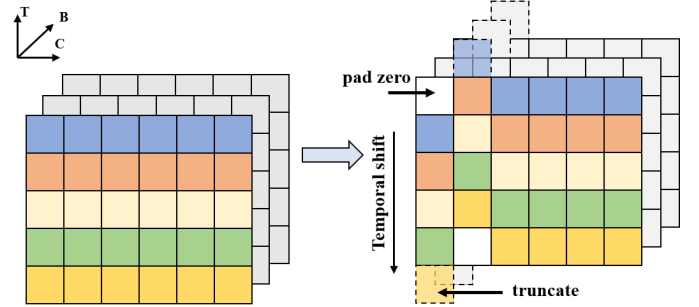


Fig. 3: **Temporal Shift operation.** **Left:** The original input feature map with dimensions of Time ( $T$ ), Batch ( $B$ ), and Channel ( $C$ ). **Right:** The transformed feature map after shifting specific channels along the temporal axis. Empty slots at the top are zero-padded, while the overflow at the bottom is truncated to preserve sequence length, facilitating local information exchange without additional parameters.

local prosodic cues. Ultimately, this encoder outputs a robust, low-dimensional feature sequence  $X_{conv}$ , establishing a stable foundation for the subsequent global attention mechanism.

#### D. Spiking Sparse Linear Attention

While the Temporal Shift Spiking Encoder effectively extracts local prosodic features, comprehending complex emotional states requires explicit modeling of long-range global dependencies. To achieve this efficiently, we design the SSLA module, whose detailed internal structure is illustrated in the bottom panel of Figure 2. This component synergizes prompt-based sequence augmentation with a linearized attention mechanism to aggregate global context while minimizing computational complexity.

We initiate the process by introducing a set of learnable prompt vectors  $\mathbf{P} \in \mathbb{R}^{L_p \times D}$ , where  $L_p$  denotes the number

of prompt tokens acting as context queries. These prompts are concatenated along the temporal dimension of the encoder output  $\mathbf{X}_{enc} \in \mathbb{R}^{T \times D}$  to construct an extended joint sequence  $\tilde{\mathbf{X}}$ :

$$\tilde{\mathbf{X}} = \text{Concat}(\mathbf{P}, \mathbf{X}_{enc}) \in \mathbb{R}^{(L_p+T) \times D} \quad (7)$$

This operation ensures that the prompts are physically embedded within the feature space, allowing them to directly participate in the subsequent feature interaction and context aggregation.

To filter background redundancy, the joint sequence  $\tilde{\mathbf{X}}$  is processed by a single-step PLIF neuron layer. Functioning as a threshold-based filter, this layer transforms continuous features into a sparse binary spike matrix  $\mathbf{S}$ . Consequently, only salient features with intensities exceeding the firing threshold are retained, while low-amplitude noise is strictly inhibited to zero:

$$\mathbf{S} = \text{PLIF}(\tilde{\mathbf{X}}) \in \{0, 1\}^{(L_p+T) \times D} \quad (8)$$

This binarization significantly reduces data density, effectively lowering the computational cost of downstream matrix operations.

Subsequently, the sparse matrix  $\mathbf{S}$  is projected into Query ( $\mathbf{Q}$ ), Key ( $\mathbf{K}$ ), and Value ( $\mathbf{V}$ ) tensors via bias-free linear layers. To circumvent the quadratic complexity  $O(L^2)$  inherent in standard Softmax attention, we employ a linearized formulation leveraging the associative property of matrix multiplication. We prioritize the computation of the global context term  $\mathbf{K}^T \mathbf{V}$ . The attention output is formally defined as:

$$\text{SSLA}(\mathbf{Q}, \mathbf{K}, \mathbf{V}) = \mathbf{Q} \cdot (\sigma(\mathbf{K})^\top \cdot \mathbf{V}) \quad (9)$$

where  $\sigma(\cdot)$  denotes the column-wise normalization function. By computing the  $D \times D$  context matrix  $\mathbf{K}^T \mathbf{V}$  first, the computational complexity is reduced to  $O((L_p+T)D^2)$ , which scales linearly with sequence length. Through this mechanism, the prompt vectors within  $\mathbf{Q}$  effectively aggregate emotion-specific semantics from the global context, yielding compact representations for the subsequent calibration stage.

### E. Context-Aware Membrane Potential Calibration

Following the SSLA stage, the output prompt sequence  $\mathbf{P}_{out}$  encapsulates the aggregated emotional context. However, these latent representations cannot directly rectify the distribution mismatch within the spiking backend. To bridge this gap, we introduce a Homeostatic Bias Generator to translate abstract context into physical voltage regulation signals. This mechanism dynamically shifts the feature baseline, aligning the input distribution with the sensitive firing range of PLIF neurons.

The calibration process commences with the derivation of a compact context descriptor  $\mathbf{c} \in \mathbb{R}^D$ . By isolating the updated prompt tokens from the joint output sequence, we perform global average pooling along the temporal axis:

$$\mathbf{c} = \frac{1}{L_p} \sum_{i=1}^{L_p} \mathbf{P}_{out}[i] \quad (10)$$

This operation effectively compresses the sequence-level semantic information into a unified global state vector, providing a holistic representation of the emotional tone.

Subsequently, the descriptor  $\mathbf{c}$  is fed into a bottleneck Multi-Layer Perceptron (MLP) to generate the dynamic bias vector  $\mathbf{v}_{bias} \in \mathbb{R}^D$ . To minimize parameter overhead while ensuring non-linear fitting capacity, the generator employs a "compress-then-expand" architecture. The mapping function is formulated as:

$$\mathbf{v}_{bias} = \kappa \cdot \tanh(\mathbf{W}_{up} \cdot \text{ReLU}(\mathbf{W}_{down} \mathbf{c} + \beta_1) + \beta_2) \quad (11)$$

Here,  $\mathbf{W}_{down} \in \mathbb{R}^{D_h \times D}$  and  $\mathbf{W}_{up} \in \mathbb{R}^{D \times D_h}$  represent the dimensionality reduction and expansion weights, respectively, where  $D_h < D$ . The tanh activation, scaled by a factor  $v_{bias}$ , enables the generation of bidirectional biases, allowing the model to exert either excitatory or inhibitory regulation.

To ensure optimization stability, we strictly constrain the initial state of the generator. We adopt a Zero Initialization strategy for the output layer parameters:

$$\mathbf{W}_{up} \leftarrow \mathbf{0}, \quad \beta_2 \leftarrow \mathbf{0} \quad (12)$$

Consequently, at the onset of training, the generated bias  $\mathbf{b}$  initializes as a zero vector. This guarantees that the model starts as an identity mapping, avoiding distributional shock caused by random initialization and facilitating a smooth transition to the adaptive state.

Finally, the generated bias  $\mathbf{v}_{bias}$  is broadcasted and injected into the original feature stream  $\mathbf{X}_{feat}$  derived from the SSLA output. The calibrated input  $\hat{\mathbf{X}}$  is defined as:

$$\hat{\mathbf{X}}[t] = \mathbf{X}_{feat}[t] + \mathbf{v}_{bias} \quad (13)$$

From a biophysical perspective, this operation introduces a context-dependent background current  $I_{bias} = \mathbf{v}_{bias}$  into the PLIF dynamics. This active regulation adaptively centers the input membrane potential around the firing threshold  $V_{th}$ , effectively preventing functional silence or saturation induced by cross-domain distribution shifts.

### F. Optimization objective

To realize end-to-end training while addressing the inherent class imbalance and label noise in SER datasets, we employ a hybrid loss function. This objective linearly combines Focal Loss, which mines hard samples, and Label Smoothing Cross-Entropy, which prevents overfitting to noisy annotations. Let  $\mathbf{o} \in \mathbb{R}^K$  denote the output vector of the SNN backend (i.e., the mean firing rate over time steps  $T$ ), where  $K$  is the number of emotion categories. The predicted probability distribution  $\mathbf{p}$  is obtained by applying the Softmax function to the output:

$$p_k = \frac{\exp(o_k)}{\sum_{j=1}^K \exp(o_j)}, \quad k \in \{1, \dots, K\} \quad (14)$$

The total optimization objective  $\mathcal{L}$  is formulated as a weighted sum of the Focal Loss term ( $\mathcal{L}_{FL}$ ) and the Label Smoothing term ( $\mathcal{L}_{LS}$ ):

$$\mathcal{L} = \lambda_1 \mathcal{L}_{FL} + \lambda_2 \mathcal{L}_{LS} \quad (15)$$

where  $\lambda_1$  and  $\lambda_2$  are hyperparameters balancing the two loss components.

**Focal Loss Term:** To mitigate the impact of class imbalance and focus the model on hard-to-classify examples, we compute the Focal Loss using the ground truth hard label  $y \in \{1, \dots, K\}$ :

$$\mathcal{L}_{FL} = -\alpha(1 - p_y)^\gamma \log(p_y) \quad (16)$$

**Label Smoothing Term:** To enhance generalization and handle label ambiguity, we construct a smoothed target distribution  $y^{ls}$ . For a target class  $y$ , the smoothed label vector is defined as:

$$y_k^{ls} = \begin{cases} 1 - \epsilon + \frac{\epsilon}{K}, & \text{if } k = y \\ \frac{\epsilon}{K}, & \text{otherwise} \end{cases} \quad (17)$$

where  $\epsilon$  is the smoothing parameter. The Label Smoothing loss is calculated as the cross-entropy between the smoothed targets and the predicted probabilities:

$$\mathcal{L}_{LS} = -\sum_{k=1}^K y_k^{ls} \log(p_k) \quad (18)$$

Based on empirical tuning, we set the focusing parameters to  $\alpha = 0.8$  and  $\gamma = 2.5$ , and the smoothing factor to  $\epsilon = 0.12$ . The loss components are weighted with  $\lambda_1 = 0.7$  and  $\lambda_2 = 0.3$  to prioritize the mining of difficult samples while maintaining regularization.

#### IV. EXPERIMENTS

This section presents a comprehensive empirical evaluation of the proposed PTS-SNN framework across five multilingual benchmark datasets. We analyze the model’s effectiveness regarding classification accuracy, parameter efficiency, and neuromorphic energy consumption, providing a detailed comparison with existing methods.

##### A. Experimental Setup

We evaluate the proposed framework on five multilingual benchmark datasets: IEMOCAP, CASIA, EMODB, EMOVO, and URDU. Detailed statistics regarding language, speaker demographics, and emotional categories are summarized in Table I. Following the protocols in emotion2vec, we adopt a leave-one-session-out 5-fold cross-validation strategy for the IEMOCAP dataset. For CASIA, we employ a random leave-one-speaker-out 4-fold cross-validation. For the remaining datasets (EMODB, EMOVO, and URDU), a random leave-one-out 10-fold cross-validation scheme is utilized to ensure rigorous evaluation.

To assess classification performance, we employ Weighted Accuracy (WA) and Unweighted Accuracy (UA). WA measures the overall accuracy across all samples, reflecting global performance. UA computes the arithmetic mean of accuracy across each class, providing a fair assessment for datasets with class imbalance.

All models were implemented using the PyTorch framework (Python 3.10.14) on a workstation equipped with a single

TABLE I: Summary of the multilingual speech emotion recognition datasets used in this study.

Dataset	Language	Speakers	Utterances	Emotions
<b>IEMOCAP</b>	English	10	5,531	4
<b>CASIA</b>	Chinese	4	1,200	4
<b>EMODB</b>	German	10	535	7
<b>EMOVO</b>	Italian	6	588	7
<b>URDU</b>	Urdu	38	400	4

NVIDIA GeForce RTX 4090 GPU (24GB VRAM). Optimization was performed using AdamW with an initial learning rate of  $2 \times 10^{-4}$  and a weight decay of 0.05. The learning rate was dynamically adjusted via a Cosine Annealing Warm Restarts scheduler, configured with an initial restart period ( $T_0$ ) of 10 epochs and a multiplication factor ( $T_{mult}$ ) of 2, decaying to a minimum of  $1 \times 10^{-6}$ . Training spanned 200 epochs with a batch size of 32. For the SNN backend, the surrogate gradient method with a steepness factor of  $\alpha_{sg} = 5$  was employed to enable backpropagation.

##### B. Main Results

**Effectiveness of Neuromorphic Adaptation.** We evaluate the adaptation strategy by comparing PTS-SNN with the emotion2vec backbone and a direct spiking baseline. As shown in Table IV, the Vanilla SNN, which directly projects continuous features into spiking neurons, yields a Weighted Accuracy (WA) of 41.78%. This performance drop indicates a distribution shift between the pre-trained features and the spiking domain. In contrast, PTS-SNN achieves 73.34%, surpassing the original emotion2vec backbone (71.79%). This result suggests that the proposed prompt-based calibration aligns the continuous representations with the spiking backend without performance degradation.

**Comparison with State-of-the-Art Methods.** Table II presents a comparison between PTS-SNN and recent speech emotion recognition architectures on the IEMOCAP dataset. The baselines include attention-based models (Co-attention, ENT) and shift-based networks (ShiftFormer). For MSTR, we report results based on our reproduction of the official implementation. In terms of classification accuracy, PTS-SNN (73.34%) outperforms MSTR (70.6%) and ShiftFormer (72.1%). The performance is comparable to ENT (72.43%) and DST (71.8%). Additionally, as indicated in the table, PTS-SNN maintains a lower parameter count and inference energy compared to these ANN-based baselines. A detailed analysis of computational efficiency is provided in the subsequent section.

**Cross-Lingual Generalization.** To verify the universality of the proposed method, we extended the evaluation to four non-English datasets: CASIA, EMODB, EMOVO, and URDU. The results are summarized in Table III. PTS-SNN consistently outperforms the emotion2vec baseline across all tested languages. On the German EMOVB dataset, the accuracy improves from 84.34% to 87.49%. Notable improvements are also observed on CASIA (+3.0%) and URDU (+2.75%),

TABLE II: Comparison with State-of-the-Art methods on the IEMOCAP dataset. †: Results reproduced using the official code implementation.

Model	Core Mechanism	WA (%)	UA (%)	Params (M)	Energy (mJ)
Co-attention [58]	Cross-Attention	69.80	71.05	175.30	103.40
MSTR† [59]	Multi-Scale Transformer	70.60	71.60	30.03	51.06
DST [60]	Dual-Stream Fusion	71.80	73.60	22.78	35.34
ShiftFormer [61]	Sparse Shift	72.10	72.70	9.50	16.20
ENT [62]	Efficient Transformer	72.43	73.88	8.55	6.35
<b>PTS-SNN (Ours)</b>	<b>Spiking Prompt</b>	<b>73.34</b>	<b>73.72</b>	<b>1.19</b>	<b>0.35</b>

demonstrating that the learned prompts capture language-agnostic emotional prosody rather than linguistic content. Even on the low-resource Italian EMOVO dataset, our method maintains a performance edge, further proving its robustness in diverse acoustic environments.

TABLE III: Cross-lingual performance comparison (WA %) on CASIA, EMOVB, EMOVO, and URDU datasets.

Dataset	Language	emotion2vec	PTS-SNN (Ours)
<b>CASIA</b>	Chinese	69.20	<b>72.50</b>
<b>EMOVB</b>	German	84.34	<b>87.49</b>
<b>EMOVO</b>	Italian	61.21	<b>61.94</b>
<b>URDU</b>	Urdu	81.50	<b>84.25</b>

TABLE IV: Performance comparison of different adaptation strategies on the IEMOCAP dataset.

Model	Adaptation Strategy	WA (%)
<b>emotion2vec</b> [22]	Standard ANN Fine-tuning	71.79
<b>Vanilla SNN</b>	Direct Spiking Conversion	41.78
<b>PTS-SNN (Ours)</b>	Neuromorphic Prompting	<b>73.34</b>

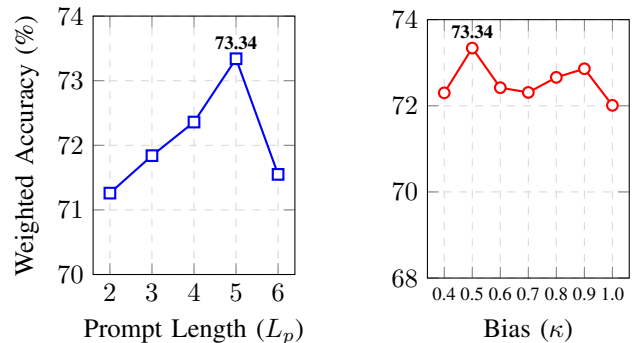
### C. Ablation Experiments

To verify the contribution of each component and analyze hyperparameter sensitivity, we conducted a series of experiments on the IEMOCAP dataset. The quantitative results of the component ablation are summarized in Table V. We first evaluate the impact of the proposed modules by removing them individually. Removing the attention module results in a performance drop from 73.34% to 68.35%, indicating that global context aggregation is critical for distinguishing complex emotional states. Similarly, replacing the learnable prompts with standard fine-tuning decreases the accuracy to 71.76%, confirming that the proposed prompting strategy adapts the frozen backbone more effectively than direct weight updates. When retaining only the temporal shift mechanism, the accuracy falls further to 61.27%, suggesting that while temporal dynamics are foundational, they are insufficient without high-level feature modulation.

We further investigate the sensitivity of the model to the prompt length ( $L_p$ ) and the bias parameter ( $b$ ) in LIF neurons.

TABLE V: Ablation study of key components on the IEMOCAP dataset. "Full Model" denotes the proposed PTS-SNN.

Configuration	WA (%)	UA (%)
<b>Full Model (PTS-SNN)</b>	<b>73.34</b>	<b>73.72</b>
w/o Prompt Tuning	71.76	71.90
w/o Attention Module	68.35	69.10
Only Temporal Shift	61.27	62.05



(a) Impact of Prompt Length (b) Impact of Bias Parameter

Fig. 4: Parameter sensitivity analysis. (a) Accuracy across different prompt lengths  $L_p$ . (b) Accuracy variations with respect to the bias parameter  $\kappa$ .

As shown in Figure 4(a), the Weighted Accuracy initially improves as  $L_p$  increases, peaking at 73.34% with  $L_p = 5$ . However, extending the length to 6 leads to a decline (71.55%), suggesting that excessive prompt tokens may introduce redundancy. Regarding the bias parameter, Figure 4(b) illustrates the performance variation across the range of  $[0.4, 1.0]$ . The accuracy reaches its optimum at  $b = 0.5$ . Values deviating from this optimal point lead to degradation; specifically, lower bias values may insufficiently activate neurons, while higher values tend to introduce noise, thereby impairing the signal-to-noise ratio of the spiking representations.

### D. Energy Consumption

Parameter Efficiency. We first evaluate model complexity regarding trainable parameters. As illustrated in Figure 5(a), PTS-SNN contains 1.19 million parameters. This low parameter count results from the adapter-based design, where the pre-trained backbone remains frozen and only the sparse spiking modules are updated. In contrast, fully fine-tuned baselines

such as MSTR and Co-attention require 30.03 M and 175.30 M parameters, respectively. Even compared to the lightweight ShiftFormer (9.50 M), our method achieves a parameter reduction of approximately 87%, facilitating deployment on memory-constrained edge devices.

**Energy Consumption.** To quantify inference costs, we adopt standard neuromorphic protocols based on 45nm CMOS technology. The energy estimation distinguishes between Multiply-Accumulate (MAC) operations in ANNs (4.6 pJ) and Accumulate (AC) operations in SNNs (0.9 pJ) [63]. We define the calculation methods for three distinct architectural paradigms as follows:

$$EC_{ANN} = MAC_s^{ANN} \times 4.6 \quad (19)$$

$$EC_{pure} = Synapsed_{activated}^{SNN} \times 0.9 \quad (20)$$

$$EC_{non-pure} = Synapsed_{activated}^{SNN} \times 0.9 + MAC_s^{ANN} \times 4.6 \quad (21)$$

Based on these formulations, the energy comparison is presented in Figure 5(b). The purely ANN-based MSTR model consumes 51.06 mJ per sample due to dense matrix computations. Similarly, ShiftFormer requires 16.20 mJ. In comparison, the proposed PTS-SNN consumes only 0.35 mJ. This significant reduction is attributed to the sparsity of the spiking dynamics, verifying the method’s suitability for power-limited applications.

## V. CONCLUSION

In this paper, we proposed PTS-SNN, a parameter-efficient neuromorphic adaptation framework designed to align frozen Self-Supervised Learning (SSL) backbones with discrete spiking dynamics for energy-efficient Speech Emotion Recognition. To effectively resolve the distributional heterogeneity that typically degrades neuronal coding capacity, the architecture integrates a Temporal Shift Spiking Encoder, which captures local temporal dependencies via parameter-free channel shifts, with a Context-Aware Membrane Potential Calibration strategy. This mechanism utilizes Spiking Sparse Linear Attention to aggregate global semantic context into learnable soft prompts, generating dynamic bias voltages that regulate Parametric Leaky Integrate-and-Fire (PLIF) neurons to effectively center the input distribution within the sensitive firing range, thereby mitigating functional silence or saturation. Empirical evaluations on five multilingual datasets (IEMOCAP, CASIA, EMODB, EMOVO, and URDU) demonstrate that PTS-SNN achieves a Weighted Accuracy of 73.34% on IEMOCAP, comparable to state-of-the-art ANNs, while requiring only 1.19 million parameters and 0.35 mJ inference energy per sample. However, the current framework relies exclusively on acoustic signals, neglecting the rich complementary information available in facial expressions and textual content inherent in human communication. Future work will focus on extending this neuromorphic prompting mechanism to multimodal spiking architectures, aiming to fuse audio-visual representations for more robust emotion understanding in complex, real-world environments.

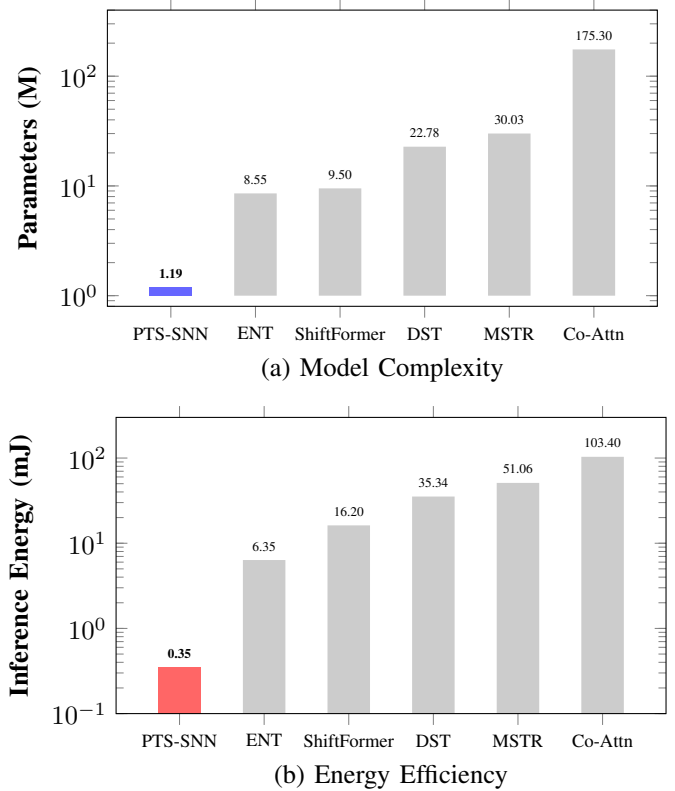


Fig. 5: Comparison of computational efficiency with state-of-the-art baselines. **(a)** Number of trainable parameters (Log scale). **(b)** Inference energy consumption per sample (Log scale). The proposed PTS-SNN demonstrates orders of magnitude improvement in both metrics.

## REFERENCES

- [1] Y. Gao, L. Wang, J. Liu, J. Dang, and S. Okada, “Adversarial domain generalized transformer for cross-corpus speech emotion recognition,” *IEEE Transactions on Affective Computing*, vol. 15, no. 2, pp. 697–708, 2023.
- [2] F. Eyben, K. R. Scherer, B. W. Schuller, J. Sundberg, E. André, C. Busso, L. Y. Devillers, J. Epps, P. Laukka, S. S. Narayanan *et al.*, “The geneva minimalistic acoustic parameter set (gemaps) for voice research and affective computing,” *IEEE transactions on affective computing*, vol. 7, no. 2, pp. 190–202, 2015.
- [3] S. Chen, C. Wang, Z. Chen, Y. Wu, S. Liu, Z. Chen, J. Li, N. Kanda, T. Yoshioka, X. Xiao *et al.*, “Wavlm: Large-scale self-supervised pre-training for full stack speech processing,” *IEEE Journal of Selected Topics in Signal Processing*, vol. 16, no. 6, pp. 1505–1518, 2022.
- [4] J. Wu, E. Yilmaz, M. Zhang, H. Li, and K. C. Tan, “Deep spiking neural networks for large vocabulary automatic speech recognition,” *Frontiers in neuroscience*, vol. 14, p. 199, 2020.
- [5] C.-K. Lu, C.-W. Lu, and G. B. Lin, “Lightweight multimodal emotion recognition for companion robots: A deep learning framework integrating facial and speech features,” *IEEE Transactions on Affective Computing*, 2025.
- [6] Z. Zhou, Y. Zhu, C. He, Y. Wang, S. YAN, Y. Tian, and L. Yuan, “Spikformer: When spiking neural network meets transformer,” in *The Eleventh International Conference on Learning Representations*, 2023.
- [7] M. Yao, J. Hu, Z. Zhou, L. Yuan, Y. Tian, B. Xu, and G. Li, “Spike-driven transformer,” *Advances in neural information processing systems*, vol. 36, pp. 64 043–64 058, 2023.
- [8] M. Bal and A. Sengupta, “Spikingbert: Distilling bert to train spiking language models using implicit differentiation,” in *Proceedings of the AAAI conference on artificial intelligence*, vol. 38, no. 10, 2024, pp. 10 998–11 006.
- [9] D. Hong and Y. Wang, “Self-attentive spatio-temporal calibration for precise intermediate layer matching in ann-to-snn distillation,” in *Pro-*



- ceedings of the AAAI Conference on Artificial Intelligence, vol. 39, no. 16, 2025, pp. 17 240–17 248.
- [10] W. Gerstner and W. M. Kistler, *Spiking neuron models: Single neurons, populations, plasticity*. Cambridge university press, 2002.
- [11] S. Wu, G. Wang, Y. Song, Y. Zhao, Y. Zhou, Q. Meng, and Y. Liao, “Bidirectional dynamic threshold snn for enhanced object detection with rich spike information,” *Frontiers in Neuroscience*, vol. 19, p. 1661916, 2025.
- [12] Y. Li, Y. Guo, S. Zhang, S. Deng, Y. Hai, and S. Gu, “Differentiable spike: Rethinking gradient-descent for training spiking neural networks,” in *Advances in Neural Information Processing Systems*, A. Beygelzimer, Y. Dauphin, P. Liang, and J. W. Vaughan, Eds., 2021.
- [13] K. Wang, J. Zhang, Y. Ren, M. Yao, D. Shang, B. Xu, and G. Li, “Spikevoice: High-quality text-to-speech via efficient spiking neural network,” in *Proceedings of the 62nd Annual Meeting of the Association for Computational Linguistics (Volume 1: Long Papers)*, 2024, pp. 7927–7940.
- [14] Z. Fu, H. Yang, A. M.-C. So, W. Lam, L. Bing, and N. Collier, “On the effectiveness of parameter-efficient fine-tuning,” in *Proceedings of the AAAI conference on artificial intelligence*, vol. 37, no. 11, 2023, pp. 12 799–12 807.
- [15] K. Yu, T. Zhang, Q. Xu, G. Pan, and H. Wang, “TS-SNN: Temporal shift module for spiking neural networks,” in *Forty-second International Conference on Machine Learning*, 2025. [Online]. Available: <https://openreview.net/forum?id=eFgtUFY6v>
- [16] X. Song, A. Song, R. Xiao, and Y. Sun, “One-step spiking transformer with a linear complexity,” in *Proceedings of the Thirty-Third International Joint Conference on Artificial Intelligence*, ser. IJCAI ’24, 2024. [Online]. Available: <https://doi.org/10.24963/ijcai.2024/348>
- [17] N. Shan, Y. Lin, C. Xie, K. Wu, W. Ma, C. Mu, X. Yan, and A. Zhang, “Membrane potential-driven adaptive threshold plasticity for snns: A bio-inspired mechanism combining inverse depolarization rate and proportional membrane potential dynamics,” *IEEE Transactions on Emerging Topics in Computational Intelligence*, 2025.
- [18] K. Takala, W. Thamviset, and S. Wongthanavas, “Biasnn: a biologically inspired attention mechanism in spiking neural networks for image classification,” *Scientific Reports*, vol. 15, no. 1, p. 38753, 2025.
- [19] W. Fang, Z. Yu, Y. Chen, T. Masquelier, T. Huang, and Y. Tian, “Incorporating learnable membrane time constant to enhance learning of spiking neural networks,” in *Proceedings of the IEEE/CVF international conference on computer vision*, 2021, pp. 2661–2671.
- [20] Z. Gong, P. Shi, K. Donbekci, L. Ai, R. Chen, D. Sasu, Z. Wu, and J. Hirschberg, “Learning More with Less: Self-Supervised Approaches for Low-Resource Speech Emotion Recognition,” in *Interspeech 2025*, 2025, pp. 151–155.
- [21] A. Baevski, Y. Zhou, A. Mohamed, and M. Auli, “wav2vec 2.0: A framework for self-supervised learning of speech representations,” *Advances in neural information processing systems*, vol. 33, pp. 12 449–12 460, 2020.
- [22] Z. Ma, Z. Zheng, J. Ye, J. Li, Z. Gao, S. Zhang, and X. Chen, “emotion2vec: Self-supervised pre-training for speech emotion representation,” in *Findings of the Association for Computational Linguistics: ACL 2024*, 2024, pp. 15 747–15 760.
- [23] S. Latif, R. Rana, S. Khalifa, R. Jurdak, J. Qadir, and B. Schuller, “Survey of deep representation learning for speech emotion recognition,” *IEEE Transactions on Affective Computing*, vol. 14, no. 2, pp. 1634–1654, 2023.
- [24] F. D’Asaro, J. J. Márquez Villacís, and G. Rizzo, “Transfer learning of large speech models for italian speech emotion recognition,” in *2024 IEEE 18th International Conference on Application of Information and Communication Technologies (AICT)*, 2024, pp. 1–6.
- [25] Y. Zhao, K. Wang, Q. Dong, and T. Ko, “Parameter-efficient transfer learning for end-to-end speech translation,” in *Proceedings of the 2024 Joint International Conference on Computational Linguistics, Language Resources and Evaluation (LREC-COLING 2024)*, 2024, pp. 12 592–12 598.
- [26] D. Yu, C. Lv, X. Du, L. Jiang, Q. Yin, W. Tong, X. Zheng, and S. Deng, “Cost-effective on-device sequential recommendation with spiking neural networks,” in *Proceedings of the Thirty-Fourth International Joint Conference on Artificial Intelligence*, 2025, pp. 3579–3587.
- [27] H. Xu, X. Qiu, Y. Xu, M. E. Elbtity, P. Zhou, Y. Tian, R.-J. Zhu, J. Zhang, S. Gu, Y. Pan *et al.*, “Neuromorphic spike-based large language model,” *National Science Review*, p. nwaf551, 2025.
- [28] M. Yao, O. Richter, G. Zhao, N. Qiao, Y. Xing, D. Wang, T. Hu, W. Fang, T. Demirci, M. De Marchi *et al.*, “Spike-based dynamic computing with asynchronous sensing-computing neuromorphic chip,” *Nature Communications*, vol. 15, no. 1, p. 4464, 2024.
- [29] A. Zhang, J. Shi, J. Wu, Y. Zhou, and W. Yu, “Low latency and sparse computing spiking neural networks with self-driven adaptive threshold plasticity,” *IEEE Transactions on Neural Networks and Learning Systems*, 2023.
- [30] T. Feng and S. Narayanan, “Peft-ser: On the use of parameter efficient transfer learning approaches for speech emotion recognition using pre-trained speech models,” in *2023 11th International Conference on Affective Computing and Intelligent Interaction (ACII)*. IEEE, 2023, pp. 1–8.
- [31] S. Deng, Y. Wu, K. Du, and S. Gu, “Spiking token mixer: An event-driven friendly former structure for spiking neural networks,” *Advances in Neural Information Processing Systems*, vol. 37, pp. 128 825–128 846, 2024.
- [32] N. Abuhajar, Z. Wang, M. Baltés, Y. Yue, L. Xu, A. Karanth, C. D. Smith, and J. Liu, “Three-stage hybrid spiking neural networks fine-tuning for speech enhancement,” *Frontiers in Neuroscience*, vol. 19, p. 1567347, 2025.
- [33] L. Qiutian, “Lightweight computational model for keyword spotting,” in *2024 21st International Computer Conference on Wavelet Active Media Technology and Information Processing (ICCWAMTIP)*. IEEE, 2024, pp. 01–05.
- [34] A. Bittar and P. N. Garner, “Exploring neural oscillations during speech perception via surrogate gradient spiking neural networks,” *Frontiers in neuroscience*, vol. 18, p. 1449181, 2024.
- [35] C. A. Buscicchio, P. Górecki, and L. Caponetti, “Speech emotion recognition using spiking neural networks,” in *International Symposium on Methodologies for Intelligent Systems*. Springer, 2006, pp. 38–46.
- [36] C. Revathy and R. Sureshbabu, “Effective technique for noise removal and emotion recognition in speech signals using cat swarm optimized spiking neural networks,” *Fluctuation and Noise Letters*, vol. 21, no. 02, p. 2250019, 2022.
- [37] E. Liebenthal, D. A. Silbersweig, and E. Stern, “The language, tone and prosody of emotions: neural substrates and dynamics of spoken-word emotion perception,” *Frontiers in neuroscience*, vol. 10, p. 506, 2016.
- [38] S. P. Mishra, P. Warule, and S. Deb, “Speech emotion recognition using spectral images and convolutional neural network,” in *2023 IEEE 20th India Council International Conference (INDICON)*. IEEE, 2023, pp. 161–166.
- [39] S. R. Gudivaka, P. Polipogu, R. Kodali, V. R. Dhulipalla, V. S. K. Tatavarty, J. Penumudi, and P. R. Gogulamudi, “Speech emotion recognition in adults and children: a comprehensive review of traditional features and raw waveform models,” *International Journal of Speech Technology*, vol. 29, no. 1, p. 21, 2026.
- [40] C. Du, F. Liu, B. Kang, and T. Hou, “Speech emotion recognition based on spiking neural network and convolutional neural network,” *Engineering Applications of Artificial Intelligence*, vol. 147, p. 110314, 2025.
- [41] X. Wang, D. Zhu, and J. Li, “A fast and accurate ann-snn conversion algorithm with negative spikes,” in *Proceedings of the Thirty-Fourth International Joint Conference on Artificial Intelligence*, 2025, pp. 6460–6468.
- [42] T. Brown, B. Mann, N. Ryder, M. Subbiah, J. D. Kaplan, P. Dhariwal, A. Neelakantan, P. Shyam, G. Sastry, A. Askell *et al.*, “Language models are few-shot learners,” *Advances in neural information processing systems*, vol. 33, pp. 1877–1901, 2020.
- [43] P. Liu, W. Yuan, J. Fu, Z. Jiang, H. Hayashi, and G. Neubig, “Pre-train, prompt, and predict: A systematic survey of prompting methods in natural language processing,” *ACM computing surveys*, vol. 55, no. 9, pp. 1–35, 2023.
- [44] B. Lester, R. Al-Rfou, and N. Constant, “The power of scale for parameter-efficient prompt tuning,” in *Proceedings of the 2021 Conference on Empirical Methods in Natural Language Processing*. Association for Computational Linguistics, 2021.
- [45] M. U. Khattak, H. Rasheed, M. Maaz, S. Khan, and F. S. Khan, “Maple: Multi-modal prompt learning,” in *Proceedings of the IEEE/CVF conference on computer vision and pattern recognition*, 2023, pp. 19 113–19 122.
- [46] J. Liang, X. Liu, W. Wang, M. D. Plumbley, H. Phan, and E. Benetos, “Acoustic prompt tuning: Empowering large language models with audition capabilities,” *IEEE Transactions on Audio, Speech and Language Processing*, 2025.
- [47] H. Xu, L. Liu, T. Liu, S. Zhi, S. Sun, and M.-M. Cheng, “Step-wise distribution-aligned style prompt tuning for source-free cross-domain few-shot learning,” *IEEE Transactions on Pattern Analysis and Machine Intelligence*, 2025.
- [48] Z. Li, T. Gao, Y. An, T. Chen, J. Zhang, Y. Wen, M. Liu, and Q. Zhang, “Brain-inspired spiking neural networks for energy-efficient

- object detection,” in *Proceedings of the Computer Vision and Pattern Recognition Conference*, 2025, pp. 3552–3562.
- [49] W. Doh, D. Lee, M. Chang, J. Mok, and S. Yoon, “Enhancing the representational power of spiking neural networks via diversified spike patterns,” 2025.
- [50] J. K. Eshraghian, M. Ward, E. O. Neftci, X. Wang, G. Lenz, G. Dwivedi, M. Bennamoun, D. S. Jeong, and W. D. Lu, “Training spiking neural networks using lessons from deep learning,” *Proceedings of the IEEE*, vol. 111, no. 9, pp. 1016–1054, 2023.
- [51] Z. Huang, W. Fang, T. Bu, P. Xue, Z. Hao, W. Liu, Y. Tang, Z. Yu, and T. Huang, “Differential coding for training-free ANN-to-SNN conversion,” in *Forty-second International Conference on Machine Learning*, 2025.
- [52] A. Islam, M. Foysal, and M. I. Ahmed, “Emotion recognition from speech audio signals using cnn-bilstm hybrid model,” in *2024 3rd International Conference on Advancement in Electrical and Electronic Engineering (ICAEEE)*. IEEE, 2024, pp. 1–6.
- [53] S. Mishra, N. Bhatnagar, P. P. and S. T. R., “Speech emotion recognition and classification using hybrid deep cnn and bilstm model,” *Multimedia Tools and Applications*, vol. 83, no. 13, pp. 37 603–37 620, 2024.
- [54] M. Li, X. Yang, and C. Deng, “Tackling long-tailed data challenges in spiking neural networks via heterogeneous knowledge distillation,” in *Proceedings of the Thirty-Fourth International Joint Conference on Artificial Intelligence*, 2025, pp. 1404–1412.
- [55] J. Gygax and F. Zenke, “Elucidating the theoretical underpinnings of surrogate gradient learning in spiking neural networks,” *Neural Computation*, vol. 37, no. 5, pp. 886–925, 2025.
- [56] Y. Kim, Y. Li, H. Park, Y. Venkatesha, A. Hambitzer, and P. Panda, “Exploring temporal information dynamics in spiking neural networks,” in *Proceedings of the AAAI conference on artificial intelligence*, vol. 37, no. 7, 2023, pp. 8308–8316.
- [57] V. Geadah, S. Horoi, G. Kerg, G. Wolf, and G. Lajoie, “Neural networks with optimized single-neuron adaptation uncover biologically plausible regularization,” *PLOS Computational Biology*, vol. 20, no. 12, p. e1012567, 2024.
- [58] H. Zou, Y. Si, C. Chen, D. Rajan, and E. S. Chng, “Speech emotion recognition with co-attention based multi-level acoustic information,” in *ICASSP 2022-2022 IEEE International Conference on Acoustics, Speech and Signal Processing (ICASSP)*. IEEE, 2022, pp. 7367–7371.
- [59] Z. Li, X. Xing, Y. Fang, W. Zhang, H. Fan, and X. Xu, “Multi-scale temporal transformer for speech emotion recognition,” *arXiv preprint arXiv:2410.00390*, 2024.
- [60] W. Chen, X. Xing, X. Xu, J. Pang, and L. Du, “Dst: Deformable speech transformer for emotion recognition,” in *ICASSP 2023-2023 IEEE International Conference on Acoustics, Speech and Signal Processing (ICASSP)*. IEEE, 2023, pp. 1–5.
- [61] S. Shen, F. Liu, and A. Zhou, “Mingling or misalignment? temporal shift for speech emotion recognition with pre-trained representations,” in *ICASSP 2023-2023 IEEE International Conference on Acoustics, Speech and Signal Processing (ICASSP)*. IEEE, 2023, pp. 1–5.
- [62] S. Shen, Y. Gao, F. Liu, H. Wang, and A. Zhou, “Emotion neural transducer for fine-grained speech emotion recognition,” in *ICASSP 2024-2024 IEEE International Conference on Acoustics, Speech and Signal Processing (ICASSP)*. IEEE, 2024, pp. 10 111–10 115.
- [63] M. Horowitz, “1.1 computing’s energy problem (and what we can do about it),” in *2014 IEEE international solid-state circuits conference digest of technical papers (ISSCC)*. IEEE, 2014, pp. 10–14.